Available online at www.sciencedirect.com

SciVerse ScienceDirect

Nuclear Medicine and Biology xx (2011) xxx–xxx

NUCLEAR MEDICINE — AND — BIOLOGY

www.elsevier.com/locate/nucmedbio

Initial evaluation in healthy humans of [^{18}F]DPA-714, a potential PET biomarker for neuroinflammation☆

Nicolas Arlicot[a,b,c,*], Johnny Vercouillie[a,b], Maria-João Ribeiro[a,b,c], Clovis Tauber[a,b], Yann Venel[c], Jean-Louis Baulieu[a,b,c], Serge Maia[b,c], Philippe Corcia[a,b,c], Michael G. Stabin[d], Aaron Reynolds[e], Michael Kassiou[e,f,g], Denis Guilloteau[a,b,c,h]

[a]*Université François Rabelais de Tours, UMR-S930 and CNRS ERL 3106, Tours, France*
[b]*Inserm, U 930, Tours, France*
[c]*CHRU Tours, Service de Médecine Nucléaire, Tours, France*
[d]*Department of Radiology and Radiological Sciences, Vanderbilt University, Nashville, Tennessee, USA*
[e]*School of Chemistry, University of Sydney, New South Wales, 2006, Australia*
[f]*Brain and Mind Research Institute, Sydney, New South Wales 2050, Australia*
[g]*Discipline of Medical Radiation Sciences, University of Sydney, New South, Wales 2006, Australia*
[h]*CIC-IT 806 Ultrasons et Radiopharmaceutiques, Tours, France*

Received 12 August 2011; received in revised form 4 October 2011; accepted 17 October 2011

Abstract

Introduction: The translocator protein 18 kDa (TSPO), although minimally expressed in healthy brain, is up-regulated in pathological conditions, coinciding with microglial activation. It is thereby a suitable in vivo biomarker of neuroinflammation for detection, evaluation and therapeutic monitoring of brain diseases. We aimed to estimate the radiation dosimetry of the positron emission tomography (PET) TSPO radioligand [^{18}F]DPA-714, and we evaluated in healthy volunteers its whole-body uptake and cerebral kinetics.

Methods: Biodistribution data from mice were used for the prediction of radiation dosimetry. In human studies, a 90-min dynamic PET scan was performed in seven healthy volunteers after injection of [^{18}F]DPA-714 (245±45 MBq). Arterial and venous samples were collected from two subjects, and two additional subjects were submitted to whole-body acquisition. Regions of interest were defined over cerebral structures to obtain mean time–activity curves and to estimate the distribution volume ratios by Logan graphical analysis, and over peripheral organs to obtain standard uptake values.

Results: The effective dose estimated from biodistribution in mice was 17.2 μSv/MBq. Modeling of regional brain and plasma data showed good in vivo stability of [^{18}F]DPA-714 in humans, with only 20% of blood metabolites 20 min postinjection (p.i.). Maximum cerebral uptake was observed 5 min p.i., followed by two decreasing phases: a rapid washout (5–30 min) followed by a slower phase for the remainder of PET acquisition. Whole-body images demonstrate high activity in the gallbladder, heart, spleen and kidneys.

Conclusions: This initial study in humans shows that [^{18}F]DPA-714 is a promising PET radioligand with excellent in vivo stability and biodistribution, and acceptable effective dose estimation. Therefore, [^{18}F]DPA-714 could provide a sensitive measure of neuroinflammatory changes in subsequent clinical investigations.

Keywords: TSPO; PET; [^{18}F]DPA-714; Biodistribution; Dosimetry; Neuroinflammation

1. Introduction

The 18-kDa translocator protein (TSPO), previously known as peripheral benzodiazepine receptor (PBR), is part of a multimeric protein complex of the outer mitochondrial membrane of many cells [1,2]. TSPO was initially characterized as a high-affinity binding site for

☆ Disclosure: The authors report no conflicts of interest. This study was supported by the EC-FP6-project DiMI, LSHB-CT-2005-512146.

* Corresponding author. Service de Médecine Nucléaire in vitro; CHRU de Tours, 2, bd Tonnellé, 37000 Tours, France. Tel.: +33 2 47 36 76 50; fax: +33 2 47 36 72 24.

E-mail address: nicolas.arlicot@univ-tours.fr (N. Arlicot).

0969-8051/$ – see front matter © 2011 Elsevier Inc. All rights reserved.
doi:10.1016/j.nucmedbio.2011.10.012

diazepam and has been demonstrated to be functionally and structurally different from the classical central benzodiazepine receptor. This protein was initially found in peripheral organs including kidneys, nasal epithelium, adrenal glands, lungs and heart.

TSPO is also minimally expressed in intact brain, where it is primarily localized in glial cells, including astrocytes and microglia [3]. Its basal expression rises in several acute and neurodegenerative disorders, including stroke [4], Alzheimer's disease [5], Parkinson's disease [6], multiple sclerosis [7], Huntington's disease [8] and amyotrophic lateral sclerosis [9], reflecting microglial activation and neuroinflammation [10]. Accordingly, TSPO is a potential target to explore in vivo neuroinflammatory changes in a variety of neurological disorders by molecular imaging [11].

Thus, the development and validation of a noninvasive TSPO biomarker would be a major advance to improve diagnosis and follow-up of therapeutic interventions. [^{11}C]-(R)-PK11195 was the first TSPO radioligand to be developed and evaluated [12,13]. However, it presented several limitations, including a relatively low bioavailability, a poor signal-to-noise ratio and high lipophilicity. Therefore, a strong impetus to produce new selective positron emission tomography (PET) TSPO radioligands occurred, and other compounds were then evaluated, including [^{11}C]DAA1106, [^{18}F]FEDAA1106, [^{11}C]PBR28 and [^{18}F]PBR06 [14–17]. Recently, a putative antagonist of TSPO, [^{11}C]-*N*,*N*-diethyl-2[2-(4-methoxyphenyl)-5,7-dimethyl-pyrazolol[1,5-α]pyrimidin-3-yl]-acetamide ([^{11}C]DPA-713), has been described [18,19]. Concurrently, the fluoro-ethoxy derivative DPA-714, a TSPO agonist, was developed and labeled with fluorine-18 [20]. Both DPA-713 and DPA-714 exhibit higher affinity for the TSPO in vitro (Ki=4.7 nM and Ki=7.0 nM, respectively) than PK11195 (Ki=9.3 nM) [18,20]. These authors reported that [^{18}F]DPA-714 showed a good uptake in the primate brain. Other groups have evaluated this radioligand in rat models of neuroinflammation, and they have concluded that it provides accurate quantitative information of the expression and distribution of TSPO after cerebral ischemia or herpes encephalitis [21–24].

As a first step to study its potential for clinical use, we performed PET measurements with [^{18}F]DPA-714 on healthy human subjects. We assessed its whole-body uptake and its cerebral kinetics, and we sought to determine its ability to quantify TSPO in the human brain. We also estimated its radiation dosimetry in humans from mice biodistribution data.

2. Material and methods

2.1. Radiopharmaceutical preparation

N,*N*-diethyl-2-(2-(4-(2-fluoroethoxy)phenyl)-5,7-dimethylpyrazolo[1,5-α]pyrimidin-3-yl)acetamide (DPA-714) was labeled with fluorine-18 at its 2-fluoroethyl moiety following nucleophilic substitution of the corresponding tosylate analogue according to slight modifications of previously reported procedures [20]. The process involved reaction of [^{18}F] KF Kryptofix-222 with the tosyloxy precursor (2.0 to 2.5 mg, 3.6 to 4.5 mmol) at 85°C for 10 min in acetonitrile (3 ml). A prepurification was performed by passing the crude reaction mixture through a *t*C18 Sep Pack cartridge. Radioactivity was eluted from the cartridge with 1 ml of acetonitrile which was sent to a high-performance liquid chromatography (HPLC) system for purification. HPLC was performed on a semipreparative Waters X-Terra column (250×10 mm) using acetonitrile/0.1 M ammonium acetate (40/60 v/v) as mobile phase (flow: 4 ml/min). [^{18}F]DPA-714 was collected, diluted with water and trapped on a *t*C18 Sep Pack cartridge. [^{18}F]DPA-714 was eluted by injectable ethanol, and saline was added to obtain an intravenously injectable solution (10% maximum in volume for ethanol). Typically, 1.4 to 2.4 GBq of [^{18}F] DPA-714 was routinely obtained with a radiochemical purity >98% ranging from 45 to 120 GBq/μmol within 75 to 85 min (HPLC purification and formulation included), starting from 20 GBq of [^{18}F] fluoride (overall non-decay-corrected yield: 7%–12%). Before being injected, the solution passed through a Millex-GV sterilizing PVDF 33-mm 0.22-μm syringe filter. The formulation of [^{18}F]DPA-714, leading to a sterile injectable solution of isotonic sodium chloride with ethanol in a percentage in mass of less than 8%, for a total injected volume ranging from 3 to 5 ml was in accordance with the European Pharmacopoeia.

2.2. Human subjects

All studies were conducted according to the French legislation and European directives. The "Ethics Committee of Tours-Région Centre Ouest I" approved this study, and seven healthy volunteers (2 male and 5 female; age 40–68 years; weight 51–80 kg) gave their written informed consent for participation. The subjects were free of medical illness (brain, heart and psychiatric diseases) on the basis of screening by medical history and physical examination. Participants had to have no contraindications to magnetic resonance imaging (MRI), which included metallic implants or prostheses, prohibitive claustrophobia and pacemakers; and for women of childbearing potential, a negative serum pregnancy test less than 7 days before the PET study had to be demonstrated. Exclusion criteria included current or past opportunistic central nervous system (CNS) infection at entry; history or current evidence of schizophrenia or depression; current severe affective disorder believed to explain the patient's cognitive impairment; history of chronic neurologic and psychiatric disorder, such as multiple sclerosis or epilepsy, or structural CNS abnormality such as stroke or arteriovenous malformation; history of head injury with loss of consciousness for over 1 h. They had to be free of vascular diseases such as diabetes, high vascular tension and dyslipidemia. Finally, subjects had to be free of anti-inflammatory/antibiotic drugs at least 1 month before the study.

2.3. Imaging data acquisition

2.3.1. MRI

Brain MRI was obtained for all subjects using a 1.5-T imager (GE Healthcare). T2-weighted images from each subject were used to reveal hypothetical brain lesions. In addition, a T1-weighted spoiled gradient recalled acquisition with inversion recovery was performed to allow a three-dimensional (3D) reconstruction of MR images.

2.3.2. PET

Subjects were examined using a Dual Gemini (Philips Medical Systems), a whole-body hybrid PET-CT scanner. The Dual Gemini is an open PET-CT system that combines a helical dual slice CT and a 3D PET scanner equipped with its own transmission source. This tomograph works exclusively in 3D detection mode (no septa). It is composed of 29 arrays of 616 gadolinium oxyorthosilicate crystals each. The axial field of view is 180 mm, and patient port is 63 cm. Acquisition data were processed with the standard package delivered with the system (Petview software, Philips Medical Systems). For cerebral studies, a low-dose CT helical scan was performed first (scan field of 600 mm, increment of 5 mm, slice thickness 3.2 mm, pitch of 1.5, 0.75 s per rotation, matrix 512×512, 120 KV, 80 mA). All cerebral PET examinations were acquired in list mode over 90 min following intravenous injection of 245±45 MBq (range 193–304 MBq), corresponding to an injected mass of 1.6 to 4.9 μg, of [^{18}F]DPA-714 and rebinned into 45 frames. Two subjects were submitted to a whole-body acquisition from the head to the hip (3 min per step) 1 h after the radiotracer injection using the same tomography. All reconstructions with attenuation correction were performed with Row-Action Maximum Likelihood Algorithm 3D iterative algorithm. Voxel size after reconstruction was 2×2×2 mm^3 for brain imaging and 4×4×4 mm^3 for whole-body acquisition [25–27].

2.4. Blood collection

For evaluation of plasmatic kinetics, 22 arterial blood samples were taken from two subjects throughout the PET acquisition. In addition, five large venous samples were also collected at 10, 20, 30, 60 and 90 min to characterize radiolabeled metabolites in plasma. Blood sampling times were recorded manually. For each blood sample and each corresponding plasma sample obtained by centrifugation (5 min at 5000 rpm), the amount of radioactivity was counted with an automatic gamma counter (Cobra Quantum Packard). The time difference between the start of the image acquisition and the start of the counting was recorded and used to correct the sample data measurements for physical decay to the start time of the PET scan. A reverse-phase HPLC method was used to determine the percentage of radioactivity in plasma corresponding to unchanged radioligand and radiometabolites during the course of the PET measurement. The plasma (0.7 ml) obtained after centrifugation of blood at 5000*g* for 5 min was mixed with acetonitrile (0.7 ml). The supernatant acetonitrile–plasma mixture was obtained after centrifugation at 2000*g* for 2 min, and a standardized volume of 0.5 ml was analyzed by HPLC [Waters column Waters X-Terra RP18 μm, 3.9×300 mm; mobile phase acetonitrile/0.1 M ammonium acetate (40/60 v/v, 1 ml/min)]. Peaks for radioactive compounds eluting from the column were integrated, and their areas were expressed as a percentage of the sum of the areas of all detected radioactive compounds (decay corrected).

2.5. PET data analysis

2.5.1. Brain studies

To evaluate the cerebral kinetics of [^{18}F]DPA-714, PET images were co-registered toward the Talairach referential with PMOD 3.2. In order to construct time–activity curves of [^{18}F]DPA-714, PET images were analyzed with the regions of interest (ROIs) for frontal, temporal and occipital cortex, striatum, thalamus and pons as defined in the Montreal Neurological Institute - Anatomical Automatic Labeling Atlas (MNI-AAL) atlas. Each regional time–activity curve was expressed as an average of the left and right regions. To evaluate the binding potential of [^{18}F]DPA-714, the PET images were quantitatively analyzed using Logan graphical analysis with the cerebellum as the reference region for time points between 0 and 90 min [28]. The distribution volume ratio (DVR) of the tracer was calculated as the slope of the linear portion of the Logan plot (at 9 min after radiotracer injection). DVR parametric images were generated, and each regional DVR was expressed as an average of the left and right regions.

2.5.2. Whole-body studies

A qualitative analysis by visual inspection was performed by two investigators. A quantitative analysis was also performed using the maximal standard uptake values [SUV(s)$_{max}$], which means that the radioactivity concentration measured in each ROI was corrected by the injected dose, the subject weight and the decay radioactivity. SUV(s)$_{max}$ were calculated using ROIs drawn by an experienced nuclear physician for lungs, heart, liver, gallbladder, adrenals, abdominal area (including the upper and lower large intestine wall, as well as the small intestine), spleen, kidneys, bladder, vertebral column (cervical, dorsal and lumbar spine), salivary glands (parotids and submandibular glands) and glutei muscle.

2.6. In vivo mice biodistribution

Studies were carried out on adult male Swiss mice (Centre d'élevage René Janvier, Le Genest-Saint-Isle, France), weighing 36±1 g, in compliance with the French legislation on animal experimentation and European directives. Animals were housed in a temperature (23±0.5°C)- and humidity (43%±8%)-controlled environment under a 12-h light–dark cycle with food and water available ad libitum. A saline solution of [^{18}F]DPA-714 (2 MBq/100 μL) was intravenously injected through the penis vein. The mice (n=4–5 per time point) were euthanized by decapitation at different times (5, 30, 60, 240 and 360 min) following radioligand injection, and organ samples, including blood,

brain, heart, adrenal, liver, kidney, gallbladder, testis, bladder and femur, were quickly removed and weighed. The radioactivity was measured with an automated γ-counter (Cobra Quantum Packard), and the percentage injected dose per gram of wet tissue(% ID/g) was calculated by comparison to a diluted standard solution derived from the initial injected solution. Radioactivity of urine absorbed on filter paper was measured and added to the bladder data; feces and large intestine contents were also collected, and their activity was measured too. All radioactivity measurements were corrected for decay.

2.7. Extrapolation to human radiation dosimetry

Biodistribution data described above were extrapolated to a reference 70-kg adult male phantom using the % kg/g mass-based extrapolation method [29] and entered into the OLINDA/EXM software. The absorbed dose in 25 target organs of the adult male phantom was estimated from the residence times of source organs by implementing the RADAR (RAdiation Dose Assessment Resource) method [30] using the OLINDA/EXM [31]. The effective dose was also calculated by OLINDA/EXM using the methodology described in Publication 60 of the International Commission on Radiological Protection [32].

3. Results

3.1. Human PET data

On the basis of patient reports, blood pressure, and heart and respiration rates, the injection of [^{18}F]DPA-714 (245±45 MBq), corresponding to an injected mass between 1.6 and 4.9 μg, did not result in either pharmacological adverse effects or subjective effects in any of the seven volunteers studied. The plasma concentration of radioactivity peaked at 1 min after [^{18}F]DPA-714 bolus injection and rapidly declined thereafter. The metabolite corrected plasma activity exhibits a similar profile (Fig. 1A). Plasma radioactivity consisted of only 20% and 35% radiometabolites at 20 and 60 min after injection, respectively (Fig. 1B).

Fig. 2 shows typical [^{18}F]DPA-714 cerebral PET images of a healthy volunteer. The activity is summed from 0 to 10 min (A), giving tracer delivery to brain, and from 30 to 90 min p.i. (B), giving retention or binding in brain. Fig. 2C presents the DVR parametric image obtained for the same subject. The uptake appeared homogeneous within the brain.

The pons exhibited the highest cerebral uptake, as confirmed by the time–activity curves presented in Fig. 3. The percentage of injected dose was about 0.02/ml of cerebral cortex. Brain uptake of radioactivity peaked within 5 min of injection, followed by two decreasing phases: a rapid decline between 5 and 30 min and then a slower phase from 30 min for the remainder of the PET acquisition. The mean±standard deviation DVR values for frontal (1.10 ±0.06), temporal (1.09±0.04) and occipital (1.08±0.09) cortex showed similar binding levels. Striatum and thalamus exhibited higher DVR values (1.16±0.04), and the highest DVR was located in the pons area (1.39±0.02).

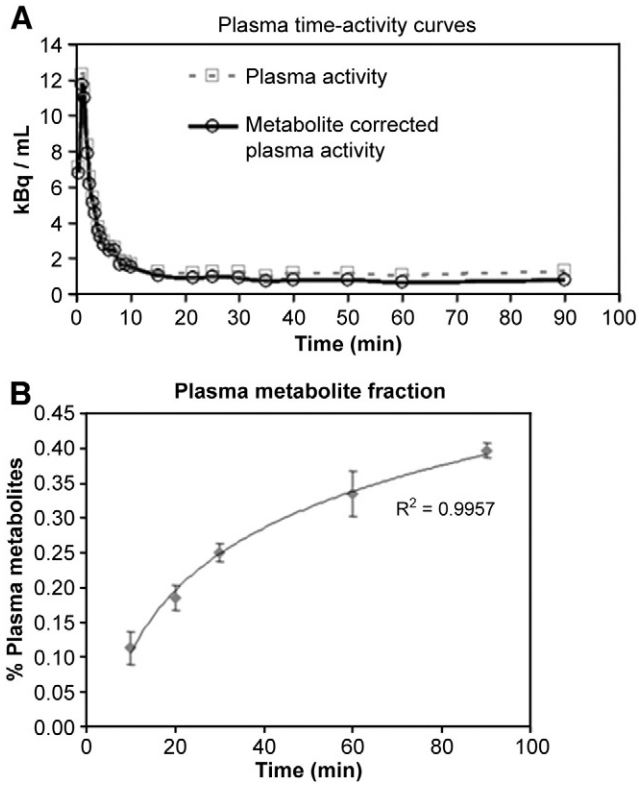

Fig. 1. Plasma metabolites concentration for [^{18}F]DPA-714 in human subjects. Plasma metabolites fraction (A) and radiometabolite-corrected plasma radioactivity (B) obtained after [^{18}F]DPA-714 injection (mean±S.D., n=2).

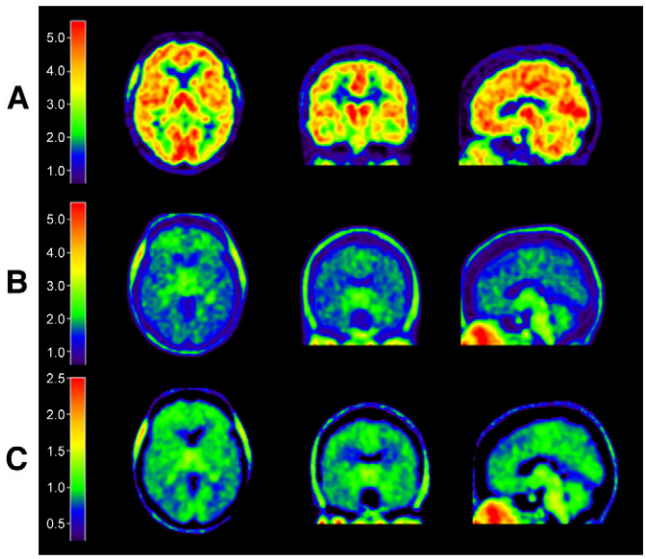

Fig. 2. Brain radioactivity distribution after bolus injection of [^{18}F]DPA-714 in healthy volunteer (injected dose: 304 MBq). (A) Integrated image from 0 to 10 min p.i.; (B) average from 30 to 90 min after injection; (C) DVR parametric image using cerebellum as nonspecific input function.

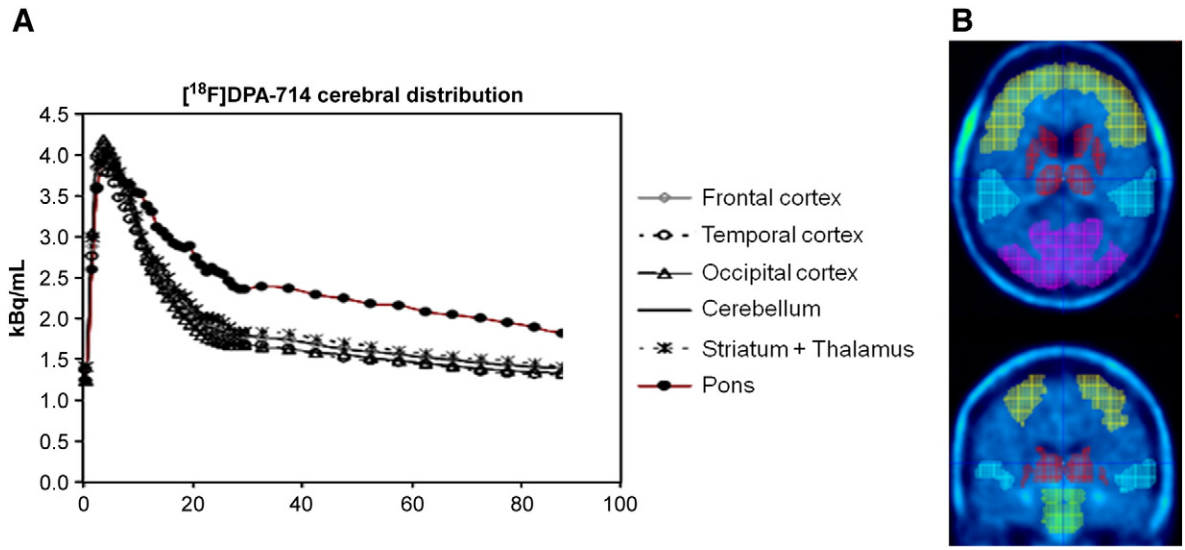

Fig. 3. Representative [18F]DPA-714 time–activity curves (kBq/ml) of [18F]DPA-714 in three cortical regions (frontal, temporal and occipital cortex), subcortical nuclei (striatum and thalamus), cerebellum and pons (A). ROIs used to obtain cerebral time–activity curves and relative distribution volume were defined in the MNI-AAL atlas and co-registered with a PET [18F]DPA-714 image (B).

Fig. 4 presents the whole-body images (coronal slices) acquired for one subject. One hour after injection, we evidenced high uptake in vertebral bodies and accumulation of activity in gallbladder. An important uptake was also observed in the heart wall, the spleen and the intestinal wall and, in an equivalent manner, in the kidneys and adrenals. The $SUV(s)_{max}$ obtained for this patient are summarized in Table 1.

3.2. In vivo mice biodistribution

The in vivo biodistribution of [18F]DPA-714 in Swiss male mice as a function of time is presented in Table 2. They were well fit with one or two exponential functions. As expected, high radioactivity accumulation was observed in peripheral tissues known to be rich in TSPO, and in most of these tissues, the maximum uptake was reached at 60 min from the injection. The adrenals displayed the highest uptake of activity of all organs with a plateau 1 to 6 h p.i. (about 60% ID/g). Heart uptake decreased over time from an initial uptake of 53.9% at 5 min to 7.0% ID/g at 6 h p.i. In the kidneys, radioactivity concentrations remained almost constant (>40% ID/g) during the first hour of the study period and decreased to less than 30% at 6 h p.i. A lower uptake was observed in other peripheral organs such as the liver and gallbladder. In the latter, the activity increased over time from 4.3% at 5 min to 12.7% ID/g at 6 h p.i. Only low concentrations of [18F]DPA-714 were found in the brain and

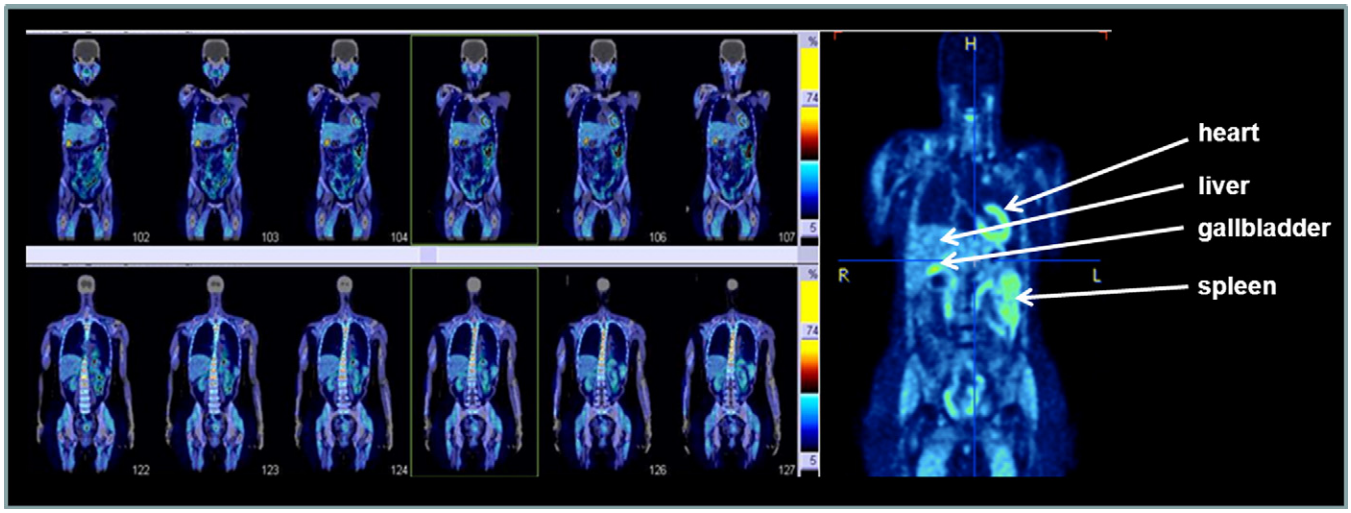

Fig. 4. Whole-body coronal PET-CT images obtained 1 h after injection of [18F]DPA-714 in a healthy volunteer (injected dose: 284 MBq). Note the high uptake by the gallbladder, the vertebral bodies and the wall heart.

Table 1
$SUV(s)_{max}$ of [^{18}F]DPA-714 obtained for one subject from dynamic whole-body PET acquisition, 1 h p.i.

Target organ	$SUV(s)_{max}$
Lungs	1.0
Heart wall	2.8
Liver	1.8
Gallbladder	5.0
Intestinal wall	2.6
Spleen	2.3
Adrenals	1.8
Kidneys	1.9
Cervical spine	2.1
Dorsal spine	3.8
Lumbar spine	3.6
Parotids	2.1
Submandibular glands	2.9
Glutei muscle	1.9

blood (≤1% ID/g) from 30 min p.i. The brain to blood concentration ratio peaked between 30 and 60 min p.i. and then decreased over time. Moreover, the femur uptake remained under 3% ID/g during the first hour, reaching 6.5% and 7.3% ID/g at 4 and 6 h p.i., respectively.

3.3. Extrapolation to human radiation dosimetry

The human radiation doses estimates (adult male model) are presented in Table 3. Most organs received from 1 to 20 μSv/MBq. The adrenals, kidneys and lungs appear to receive the highest doses, about 100, 90 and 60 μSv/MBq, respectively. The effective dose was estimated at 17.2 μSv/MBq.

4. Discussion

The current study evaluated DPA-714, labeled with fluorine-18, for both biodistribution and radiation dosimetry estimation in mice, and quantitative brain and whole-body PET imaging in healthy living human subjects. The emergence of ligands labeled with fluorine-18 is a major and necessary step towards a better understanding of the phenomena associated with neuroinflammation and their role in the pathophysiology of cerebral diseases. Indeed, fluorine-18 has physical characteristics (i.e., longer half-life and lower positron energy) more favorable than carbon-11. These advantages provide fluorine-18-labeled radiopharmaceuticals better counting statistics by extending the period of data acquisition, which may be required to measure significantly increased binding site density, and allow distribution of the radioligands to distant nuclear medicine centers, as routinely done for [^{18}F]FDG, whereas carbon-11 half-life (20.4 min) restricts its use exclusively to centers equipped with a cyclotron.

Table 2
Distribution of [^{18}F]DPA-714 in mice

Percent ID/g	5 min	30 min	60 min	240 min	360 min
Blood	2.5±0.5	0.4±0.1	0.5±0.1	0.8±0.1	0.8±0.1
Brain	3.3±0.4	1.0±0.2	0.8±0.1	0.7±0.1	0.8±0.1
Heart	53.9±5.9	23.8±3.5	17.4±2.8	7.6±0.5	7.0±0.5
Adrenal	37.0±2.7	37.0±8.3	66.0±7.1	53.3±3.5	62.1±1.9
Liver	6.4±0.5	9.4±1.0	12.1±1.8	9.8±0.6	8.8±1.0
Kidney	40.2±6.2	40.2±6.5	45.7±7.6	30.4±2.0	27.1±2.9
Gallbladder	4.3±1.5	4.6±1.0	8.9±0.8	13.6±1.3	12.7±1.6
Testis	1.3±0.2	1.2±0.2	1.6±0.4	1.8±0.1	1.8±0.2
Femur	2.0±0.3	2.6±0.3	2.9±0.3	6.5±0.5	7.3±0.4

Results are mean±S.D. % ID/g.

Table 3
Human radiation doses estimates of [^{18}F]DPA-714 from a tissue dissection study in mice

Target organ	Estimated dose (μSv/MBq)	Target organ	Estimated dose (μSv/MBq)
Adrenals	96.8	Ovaries	4.47
Brain	4.17	Pancreas	8.63
Breasts	4.13	Red marrow	9.03
Gallbladder wall	22.6	Osteogenic Cells	18.1
Lower large intestine wall	7.21	Skin	1.92
Small intestine	1.84	Spleen	5.91
Stomach wall	5.14	Testis	1.04
Upper large intestine wall	21.2	Thymus	5.20
Heart wall	44.3	Thyroid	2.04
Kidneys	89.7	Urinary bladder wall	131
Liver	45.1	Uterus	3.97
Lungs	64.1	Total body	6.63
Muscle	3.40	Effective dose	17.2

Effective dose was calculated according to Publication 60 of the International Commission on Radiological Protection [32].

The in vivo biodistribution and dosimetry of [^{18}F]DPA-714 have been performed in mice. [^{18}F]DPA-714 rapidly accumulated in TSPO-rich tissues such as the heart, kidneys and adrenals, and at a lower level in the brain, which was further confirmed by PET human whole-body images. It was in agreement with previous findings on TSPO localization in the peripheral systems of rodents [33,34], with high density in endocrine tissues such as the adrenal glands [3], and in peripheral organs such as the kidney [35] and heart [36]. Uptake in the heart may be related to calcium metabolism since TSPO is coupled to calcium channels in this organ [37]. Moreover, the decreasing kinetic of heart activity included a blood flow part of the [^{18}F]DPA-714 distribution. Conversely, the activity increased over time in gallbladder, suggesting a gastrointestinal elimination of the compound. The uptake of [^{18}F]DPA-714 was also in accordance with the distribution of [^{11}C]-(R)-PK11195 in mouse [38].

The effective dose of [^{18}F]DPA-714, extrapolated from the animal biodistribution results, was 17.2 μSv/MBq. This dose level for [^{18}F]DPA-714 was half of that recently estimated in human for FEDAA1106 (36 μSv/MBq) [39], but similar to that measured in human for PBR06 (18.5 μSv/

MBq) [40], two other TSPO [^{18}F]-labeled radioligands, whereas it was about three times more than the one established for PK11195 and PBR28, both radiolabeled with carbon-11, for which effective dose was estimated between 4 and 7 μSv/MBq [41,42]. This concordance may be related to the fact that the majority of dosimetric studies of tracers labeled with fluorine-18 showed that residence times and the effective dose depend more on the physical half-life than biological half-life. Therefore, our data provide a reasonable basis for predicting the approximate human dosimetry of [^{18}F]DPA-714. This point might be of course better established in human subjects, but it could not have been reached for ethical purpose in the present study since whole-body scans were performed at a single time point.

Having confirmed the radiation safety of [^{18}F]DPA-714, we sought to evaluate its ability to quantify TSPO in human brain. This initial evaluation of [^{18}F]DPA-714 in healthy subjects, the first in-human use of [^{18}F]DPA-714, demonstrated a favorable biodistribution of the tracer with a percentage of injected activity being about 0.02/ml for the cerebral cortex. The maximum brain extraction fraction was observed between 2 and 6 min p.i., followed by two decrease phases: a first washout between 6 and 30 min, during which the cerebral cortex, striatal and thalamic activity concentration rapidly decreased, and, from 30 min to the end of the PET acquisition, a slower decline of the activity concentration. Regarding the low density of TSPO in the normal brain, the second phase clearance might be a mixture of nonspecific binding and free tracer in the brain. We observed a fast decrease to 50% of the cerebral peak uptake by 30 min p.i. and to 33% of the peak at 90 min, quite similar to that detected for the carbon-11-labeled analogue of [^{18}F]DPA-714, [^{11}C]DPA-713 [19]. In this study, Endres and colleagues compared in healthy volunteers brain uptake of [^{11}C]DPA-713 with that of [^{11}C]-(R)-PK11195 and concluded that [^{11}C]DPA-713 has excellent brain uptake and provided a higher brain signal than [^{11}C]-(R)-PK11195. The biodistribution of [^{18}F]DPA-714 was also in good agreement with previous reports of fluorine-18-radiolabeled tracers in human brain. Thus, intravenous injection of [^{18}F]PBR06 showed radioactivity to peak in the brain at 3 min, followed by a 50% decrease of the peak 1 h p.i. [40,43]. As expected from the known distribution of TSPO in the human brain, the activity biodistribution was widespread and relatively identical in the different cerebral cortical regions, cerebellum and deep brain nuclei [44]. However, the activity concentration in the pons always remained higher than that in the other cerebral regions throughout the PET study. This is in accordance with the known distribution of TSPO in the central nervous system and particularly in the pons [45,46] as confirmed by other PET studies showing high TSPO binding in this brain area [19,46,47]. A limitation of our study may be the use of cerebellum as a reference tissue [44]. However, several authors have compared cerebellum and plasma radioactivity concentration as input function and Logan graphical analysis for quantification of the binding of other TSPO radioligands, including [^{11}C]-(R)-PK11195 [47–50]. They compared cerebellum and cluster analysis and have shown that potential binding values were reasonably well correlated [48–50]. Our results showed that DVR values, using cerebellum as reference tissue, were lower but quite homogeneous for cortical regions and higher for the pons, in accordance with results obtained for [^{11}C]DPA-713 [19] and [^{11}C]-(R)-PK11195 [47]. However, an increase of specific binding in the cerebellum, associated with aging even in normal brain [51], may result in underestimation of specific binding in target regions. Therefore, only "middle-aged" control subjects (40–68 years old), with presumably minimal glial activity and thus minimal TSPO binding, were included in the present study.

The formation of blood radiometabolites was relatively low (20% of plasma activity due to radiometabolites at 20 min p.i.) and comparable to that observed for |^{11}C]DPA-713 [19]. For these two pyrazolopyrimidine derivatives, the percentage of radiometabolites was lower than that observed for [^{11}C]-(R)-PK11195, with about 40% of radiometabolites observed at 20 min [19] and 55% at 1 h p.i. [19,52]. Two classes of organs were visually identified with moderate to high levels of activity on whole-body PET-CT images obtained 1 h after [^{18}F]DPA-714 injection: those with high densities of TSPO and those involved with metabolism and excretion pathways. Indeed, distribution of radioactivity was consistent with the known gene expression distribution of TSPO: we observed a high uptake of [^{18}F]DPA-714 in TSPO-rich organs (kidneys, spleen, heart), as well as glandular and secretory tissues such as salivary glands and olfactory epithelium. These results are in accordance with autoradiographic studies performed with either of the selective TSPO tritium-labeled ligands Ro5-4864 or PK11195 [2,33]. Moreover, the accumulation of activity in gallbladder suggests an at least partial elimination of [^{18}F]DPA-714 by the hepatobiliary system. Finally, we observed [^{18}F]DPA-714 vertebral uptake in the spinal cord, whereas bone had relatively little uptake, suggesting negligible defluorination in vivo. This accumulation of activity in bones with high marrow content has already been described with [^{11}C]-(R)-PK11195 in animal [53] as well as human [41] studies.

A recent publication demonstrated the existence of different binder populations for the [^{11}C]PBR28, for which about 10% of the population appeared to be nonbinders [54]. Owen and colleagues [55] evidenced three types of binding pattern: high-affinity binders (~50%), low-affinity binders (~20%) and mixed-affinity binders (~30%), and extended this finding to other PET TSPO radioligands, including the carbon 11-radiolabeled derivative of [^{18}F]DPA-714, namely, DPA-713. Although we have not directly identified a subject with low affinity for TSPO in the present study, including only seven healthy controls, it is likely that [^{18}F]DPA-714 is also sensitive to this interindividual variable affinity state. Therefore, the existence of different binder populations requires the knowledge of the "binding pattern" of patients

for any dedicated TSPO radiotracer to accurately quantify TSPO expression in brain in further clinical PET studies.

5. Conclusion

On the basis of animal biodistribution data, [^{18}F]DPA-714 exhibited a radiation exposure similar to other fluorine-radiolabeled tracers, with an effective dose of 17.2 μSv/MBq. The initial evaluation in healthy human subjects of this promising PET radioligand to image TSPO, a marker of neuroinflammation, showed that the regional distribution of [^{18}F]DPA-714 was in good agreement with previous PET studies using TSPO ligands in the human brain. With these data, future studies can be expanded into the clinical setting to test the usefulness of [^{18}F]DPA-714 in the diagnosis and monitoring of neurologic diseases associated with microglial activation.

Acknowledgments

This work was financially supported in part by the ECFP6-project DiMI, LSHB-CT-2005-512146, and by Région Centre and FEDER: "Radex" programme. We thank the technician and nursing staff of the CERRP, the Service de Médecine Nucléaire, CHRU Tours and the CIC-IT for their assistance.

References

[1] Papadopoulos V, Baraldi M, Guilarte TR, Knudsen TB, Lacapere JJ, Lindemann P, et al. Translocator protein (18kDa): new nomenclature for the peripheral-type benzodiazepine receptor based on its structure and molecular function. Trends Pharmacol Sci 2006;27:402–9.

[2] Chen MK, Guilarte TR. Translocator protein 18 kDa (TSPO): molecular sensor of brain injury and repair. Pharmacol Ther 2008; 118:1–17.

[3] Benavides J, Quarteronet D, Imbault F, Malgouris C, Uzan A, Renault C, et al. Labelling of "peripheral-type" benzodiazepine binding sites in the rat brain by using [^{3}H]PK 11195, an isoquinoline carboxamide derivative: kinetic studies and autoradiographic localization. J Neurochem 1983;41:1744–50.

[4] Pappata S, Levasseur M, Gunn RN, Myers R, Crouzel C, Syrota A, et al. Thalamic microglial activation in ischemic stroke detected in vivo by PET and [^{11}C]PK1195. Neurology 2000;55:1052–4.

[5] Cagnin A, Brooks DJ, Kennedy AM, Gunn RN, Myers R, Turkheimer FE, et al. In-vivo measurement of activated microglia in dementia. Lancet 2001;358:461–7.

[6] Papadopoulos V, Lecanu L, Brown RC, Han Z, Yao ZX. Peripheral-type benzodiazepine receptor in neurosteroid biosynthesis, neuropathology and neurological disorders. Neuroscience 2006; 138:749–56.

[7] Banati RB, Newcombe J, Gunn RN, Cagnin A, Turkheimer F, Heppner F, et al. The peripheral benzodiazepine binding site in the brain in multiple sclerosis: quantitative in vivo imaging of microglia as a measure of disease activity. Brain 2000;123:2321–37.

[8] Messmer K, Reynolds GP. Increased peripheral benzodiazepine binding sites in the brain of patients with Huntington's disease. Neurosci Lett 1998;241:53–6.

[9] Turner MR, Cagnin A, Turkheimer FE, Miller CC, Shaw CE, Brooks DJ, et al. Evidence of widespread cerebral microglial activation in amyotrophic lateral sclerosis: an [^{11}C](R)-PK11195 positron emission tomography study. Neurobiol Dis 2004;15:601–9.

[10] Benavides J, Fage D, Carter C, Scatton B. Peripheral type benzodiazepine binding sites are a sensitive indirect index of neuronal damage. Brain Res 1987;421:167–72.

[11] Venneti S, Lopresti BJ, Wiley CA. The peripheral benzodiazepine receptor (translocator protein 18kDa) in microglia: from pathology to imaging. Prog Neurobiol 2006;80:308–22.

[12] Le Fur G, Perrier ML, Vaucher N, Imbault F, Flamier A, Benavides J, et al. Peripheral benzodiazepine binding sites: effect of PK 11195, 1-(2-chlorophenyl)-*N*-methyl-*N*-(1-methylpropyl)-3-isoquinolinecarboxamide. I. In vitro studies. Life Sci 1983;32:1839–47.

[13] Shah F, Hume SP, Pike VW, Ashworth S, McDermott J. Synthesis of the enantiomers of [*N*-methyl-^{11}C]PK 11195 and comparison of their behaviours as radioligands for PK binding sites in rats. Nucl Med Biol 1994;21:573–81.

[14] Yasuno F, Ota M, Kosaka J, Ito H, Higuchi M, Doronbekov TK, et al. Increased binding of peripheral benzodiazepine receptor in Alzheimer's disease measured by positron emission tomography with [^{11}C] DAA1106. Biol Psychiatry 2008;64:835–41.

[15] Shidahara M, Ikoma Y, Seki C, Fujimura Y, Naganawa M, Ito H, et al. Wavelet denoising for voxel-based compartmental analysis of peripheral benzodiazepine receptors with (18)F-FEDAA1106. Eur J Nucl Med Mol Imaging 2008;35:416–23.

[16] Fujimura Y, Zoghbi SS, Simeon FG, Taku A, Pike VW, Innis RB, et al. Quantification of translocator protein (18 kDa) in the human brain with PET and a novel radioligand, (18)F-PBR06. J Nucl Med 2009;50:1047–53.

[17] Imaizumi M, Briard E, Zoghbi SS, Gourley JP, Hong J, Fujimura Y, et al. Brain and whole-body imaging in nonhuman primates of [^{11}C] PBR28, a promising PET radioligand for peripheral benzodiazepine receptors. Neuroimage 2008;39:1289–98.

[18] Boutin H, Chauveau F, Thominiaux C, Gregoire MC, James ML, Trebossen R, et al. ^{11}C-DPA-713: a novel peripheral benzodiazepine receptor PET ligand for in vivo imaging of neuroinflammation. J Nucl Med 2007;48:573–81.

[19] Endres CJ, Pomper MG, James M, Uzuner O, Hammoud DA, Watkins CC, et al. Initial evaluation of ^{11}C-DPA-713, a novel TSPO PET ligand, in humans. J Nucl Med 2009;50:1276–82.

[20] James ML, Fulton RR, Vercoullie J, Henderson DJ, Garreau L, Chalon S, et al. DPA-714, a new translocator protein-specific ligand: synthesis, radiofluorination, and pharmacologic characterization. J Nucl Med 2008;49:814–22.

[21] Chauveau F, Van Camp N, Dolle F, Kuhnast B, Hinnen F, Damont A, et al. Comparative evaluation of the translocator protein radioligands [^{11}C]DPA-713, [^{18}F]DPA-714, and [^{11}C]PK11195 in a rat model of acute neuroinflammation. J Nucl Med 2009;50:468–76.

[22] Doorduin J, Klein HC, Dierckx RA, James M, Kassiou M, de Vries EF. [^{11}C]-DPA-713 and [^{18}F]-DPA-714 as new PET tracers for TSPO: a comparison with [^{11}C]-(R)-PK11195 in a rat model of herpes encephalitis. Mol Imaging Biol 2009;11:386–98.

[23] Martin A, Boisgard R, Theze B, Van Camp N, Kuhnast B, Damont A, et al. Evaluation of the PBR/TSPO radioligand [(18)F]DPA-714 in a rat model of focal cerebral ischemia. J Cereb Blood Flow Metab 2009;30:230–41.

[24] Martin A, Boisgard R, Kassiou M, Dolle F, Tavitian B. Reduced PBR/TSPO expression after minocycline treatment in a rat model of focal cerebral ischemia: a PET study using [(18)F]DPA-714. Mol Imaging Biol 2011;13:10–5.

[25] Daube-Witherspoon M, Matej S, Karp J, Lewitt R. Application of the row action maximum likelihood algorithm with spherical basis functions to clinical PET imaging. Trans Nucl Sci 2001;48:24–30.

[26] Takashi O, Matej S, Lewitt R, Gabor Herman T. 2.5 D simultaneous multislice reconstruction by series expansion methods from Fourier-rebinned PET data. IEEE Trans Med Imaging 2000;19:474–84.

[27] Browne J, De Pierro A. A row-action alternative to the EM algorithm for maximizing likelihood in emission tomography. IEEE Trans Med Imaging 1996;15:687–99.

[28] Logan J, Fowler JS, Volkow ND, Wolf AP, Dewey SL, Schlyer DJ, et al. Graphical analysis of reversible radioligand binding from time-activity measurements applied to [*N*-^{11}C-methyl]-(−)-cocaine PET studies in human subjects. J Cereb Blood Flow Metab 1990;10:740–7.

[29] Kirschner A, Ice R, Beierwaltes W. Radiation dosimetry of ^{131}I-19-iodocholesterol: the pitfalls of using tissue concentration data, the author's reply. J Nucl Med 1975;16:248–9.

[30] Stabin MG, Siegel JA. Physical models and dose factors for use in internal dose assessment. Health Phys 2003;85:294–310.

[31] Stabin MG, Sparks RB, Crowe E. OLINDA/EXM: the second-generation personal computer software for internal dose assessment in nuclear medicine. J Nucl Med 2005;46:1023–7.

[32] International Commission on Radiological Protection. ICRP publication 60: 1990 recommendations of the International Commission on Radiological Protection. Ann ICRP 1991;21:493–502.

[33] Gavish M, Bachman I, Shoukrun R, Katz Y, Veenman L, Weisinger G, et al. Enigma of the peripheral benzodiazepine receptor. Pharmacol Rev 1999;51:629–50.

[34] Anholt RR, De Souza EB, Oster-Granite ML, Snyder SH. Peripheral-type benzodiazepine receptors: autoradiographic localization in whole-body sections of neonatal rats. J Pharmacol Exp Ther 1985;233: 517–26.

[35] Gehlert DR, Stephenson DT, Schober DA, Rash K, Clemens JA. Increased expression of peripheral benzodiazepine receptors in the facial nucleus following motor neuron axotomy. Neurochem Int 1997; 31:705–13.

[36] Gildersleeve DL, Van Dort ME, Johnson JW, Sherman PS, Wieland DM. Synthesis and evaluation of [^{123}I]-iodo-PK11195 for mapping peripheral-type benzodiazepine receptors (omega 3) in heart. Nucl Med Biol 1996;23:23–8.

[37] Charbonneau P, Syrota A, Crouzel C, Valois JM, Prenant C, Crouzel M. Peripheral-type benzodiazepine receptors in the living heart characterized by positron emission tomography. Circulation 1986;73: 476–83.

[38] Hashimoto K, Inoue O, Suzuki K, Yamasaki T, Kojima M. Synthesis and evaluation of ^{11}C-PK 11195 for in vivo study of peripheral-type benzodiazepine receptors using positron emission tomography. Ann Nucl Med 1989;3:63–71.

[39] Takano A, Gulyás B, Varrone A, Karlsson P, Sjoholm N, Larsson S, et al. Biodistribution and radiation dosimetry of the 18 kDa translocator protein (TSPO) radioligand [(18)F]FEDAA1106: a human whole-body PET study. Eur J Nucl Med Mol Imaging 2011, doi:10.1007/s00259-011-1864-3.

[40] Fujimura Y, Kimura Y, Simeon FG, Dickstein LP, Pike VW, Innis RB, et al. Biodistribution and radiation dosimetry in humans of a new PET ligand, (18)F-PBR06, to image translocator protein (18 kDa). J Nucl Med 2010;51:145–9.

[41] Hirvonen J, Roivainen A, Virta J, Helin S, Nagren K, Rinne JO. Human biodistribution and radiation dosimetry of (11)C-(R)-PK11195, the prototypic PET ligand to image inflammation. Eur J Nucl Med Mol Imaging 2010;37:606–12.

[42] Brown AK, Fujita M, Fujimura Y, Liow JS, Stabin M, Ryu YH, et al. Radiation dosimetry and biodistribution in monkey and man of ^{11}C-PBR28: a PET radioligand to image inflammation. J Nucl Med 2007;48:2072–9.

[43] Dickstein LP, Zoghbi SS, Fujimura Y, Imaizumi M, Zhang Y, Pike VW, et al. Comparison of ^{18}F- and ^{11}C-labeled aryloxyanilide analogs to measure translocator protein in human brain using positron emission tomography. Eur J Nucl Med Mol Imaging 2011;38:352–7.

[44] Doble A, Malgouris C, Daniel M, Daniel N, Imbault F, Basbaum A, et al. Labelling of peripheral-type benzodiazepine binding sites in human brain with [^{3}H]PK 11195: anatomical and subcellular distribution. Brain Res Bull 1987;18:49–61.

[45] Giguere JF, Hamel E, Butterworth RF. Increased densities of binding sites for the 'peripheral-type' benzodiazepine receptor ligand [^{3}H]PK 11195 in rat brain following portacaval anastomosis. Brain Res 1992;585:295–8.

[46] Maeda J, Suhara T, Zhang MR, Okauchi T, Yasuno F, Ikoma Y, et al. Novel peripheral benzodiazepine receptor ligand [^{11}C]DAA1106 for PET: an imaging tool for glial cells in the brain. Synapse 2004;52: 283–91.

[47] Turkheimer FE, Edison P, Pavese N, Roncaroli F, Anderson AN, Hammers A, et al. Reference and target region modeling of [^{11}C]-(R)-PK11195 brain studies. J Nucl Med 2007;48:158–67.

[48] Schuitemaker A, van Berckel BN, Kropholler MA, Kloet RW, Jonker C, Scheltens P, et al. Evaluation of methods for generating parametric (R-[^{11}C]PK11195 binding images. J Cereb Blood Flow Metab 2007; 27:1603–15.

[49] Schuitemaker A, van Berckel BN, Kropholler MA, Veltman DJ, Scheltens P, Jonker C, et al. SPM analysis of parametric (R)-[^{11}C] PK11195 binding images: plasma input versus reference tissue parametric methods. Neuroimage 2007;35:1473–9.

[50] Kropholler MA, Boellaard R, Schuitemaker A, Folkersma H, van Berckel BN, Lammertsma AA. Evaluation of reference tissue models for the analysis of [^{11}C](R)-PK11195 studies. J Cereb Blood Flow Metab 2006;26:1431–41.

[51] Mrak RE, Griffin WS. Glia and their cytokines in progression of neurodegeneration. Neurobiol Aging 2005;26:349–54.

[52] Greuter HN, van Ophemert PL, Luurtsema G, van Berckel BN, Franssen EJ, Windhorst BD, et al. Optimizing an online SPE-HPLC method for analysis of (R)-[^{11}C]1-(2-chlorophenyl)-*N*-methyl-*N*-(1-methylpropyl)-3-isoquinolinecarboxamide [(R)-[^{11}C]PK11195] and its metabolites in humans. Nucl Med Biol 2005;32:307–12.

[53] Vowinckel E, Reutens D, Becher B, Verge G, Evans A, Owens T, et al. PK11195 binding to the peripheral benzodiazepine receptor as a marker of microglia activation in multiple sclerosis and experimental autoimmune encephalomyelitis. J Neurosci Res 1997;50:345–53.

[54] Kreisl WC, Fujita M, Fujimura Y, Kimura N, Jenko KJ, Kannan P, et al. Comparison of [(11)C]-(R)-PK 11195 and [(11)C]PBR28, two radioligands for translocator protein (18 kDa) in human and monkey: implications for positron emission tomographic imaging of this inflammation biomarker. Neuroimage 2010;49:2924–32.

[55] Owen DR, Gunn RN, Rabiner EA, Bennacef I, Fujita M, Kreisl WC, et al. Mixed-affinity binding in humans with 18-kDa translocator protein ligands. J Nucl Med 2011;52:24–32.